

LETTER • **OPEN ACCESS**

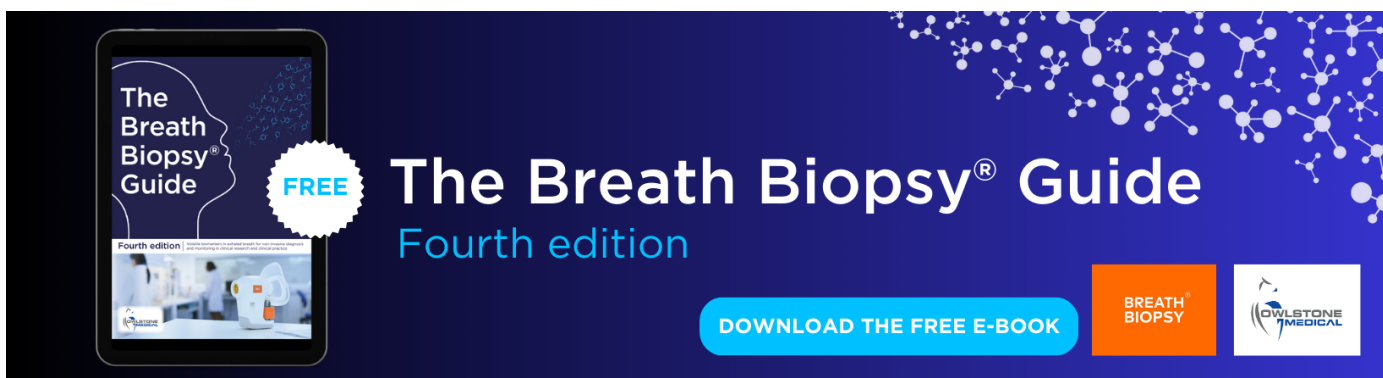
Subseasonal reversals of winter surface air temperature in mid-latitude Asia and the roles of westward-shift NAO

To cite this article: Xiaolei Song *et al* 2023 *Environ. Res. Lett.* **18** 034018

View the [article online](#) for updates and enhancements.

You may also like

- [Stratospheric initial conditions provide seasonal predictability of the North Atlantic and Arctic Oscillations](#)
Yu Nie, Adam A Scaife, Hong-Li Ren *et al.*
- [Atmospheric circulation patterns which promote winter Arctic sea ice decline](#)
Binhe Luo, Dehai Luo, Lixin Wu *et al.*
- [How do intermittency and simultaneous processes obfuscate the Arctic influence on midlatitude winter extreme weather events?](#)
J E Overland, T J Ballinger, J Cohen *et al.*



The Breath Biopsy® Guide
Fourth edition

FREE

DOWNLOAD THE FREE E-BOOK

BREATH BIOPSY

OWLSTONE MEDICAL

ENVIRONMENTAL RESEARCH
LETTERS

LETTER

Subseasonal reversals of winter surface air temperature in mid-latitude Asia and the roles of westward-shift NAO

OPEN ACCESS

RECEIVED

21 November 2022

REVISED

8 January 2023

ACCEPTED FOR PUBLICATION

31 January 2023

PUBLISHED

21 February 2023

Original content from this work may be used under the terms of the [Creative Commons Attribution 4.0 licence](https://creativecommons.org/licenses/by/4.0/).

Any further distribution of this work must maintain attribution to the author(s) and the title of the work, journal citation and DOI.

Xiaolei Song¹, Zhicong Yin^{1,2,3,*} and Yijia Zhang¹

¹ Key Laboratory of Meteorological Disaster, Ministry of Education/Joint International Research Laboratory of Climate and Environment Change (ILCEC)/Collaborative Innovation Center on Forecast and Evaluation of Meteorological Disasters (CIC-FEMD), Nanjing University of Information Science & Technology, Nanjing 210044, People's Republic of China

² Southern Marine Science and Engineering Guangdong Laboratory (Zhuhai), Zhuhai, People's Republic of China

³ Nansen-Zhu International Research Centre, Institute of Atmospheric Physics, Chinese Academy of Sciences, Beijing, People's Republic of China

* Author to whom any correspondence should be addressed.

E-mail: yinzhc@nuist.edu.cn

Keywords: subseasonal reversal, surface air temperature, Ural blocking high, Scandinavia teleconnection, NAO, North Atlantic jet stream

Supplementary material for this article is available [online](#)

Abstract

Reversals of surface air temperature anomalies over mid-latitude Asia (SAT_{MA}) have become more frequent. Six winters have been reversed over the last decade, which had serious negative consequences for agricultural production, ecological systems, and human health. This subseasonal reversal can be observed in the second mode of season-reliant empirical orthogonal function analysis, showing a persistent opposite anomaly between early and late winter. The difference in SAT_{MA} between early and late winter exceeds $3\text{ }^{\circ}\text{C}$ when the reversal occurs. At the time of the reversal, the North Atlantic jet stream extends eastward in early winter and recedes westward in late winter. The main influencing system changes from the Scandinavia teleconnection to the Ural blocking high, accompanied by a change from strong southerly to northerly winds. These factors jointly lead to the reversal of SAT_{MA} between early and late winter. More importantly, the North Atlantic Oscillation (NAO) has been shown to affect SAT_{MA} variability in a variety of different ways. Changes in SAT_{MA} are influenced not only by the intensity of the NAO, but also by its spatial distribution. When the southern center of the NAO shifts westward and is located over the North Atlantic, atmospheric circulation and SAT_{MA} in early and late winter show similar changes to those seen in SAT_{MA} reversal winters. In contrast, when the NAO southern center shifts eastward and is located over Western Europe, persistent anomalies are observed in atmospheric circulation and SAT_{MA} throughout the winter. Therefore, when studying the relationship between SAT_{MA} and the NAO, attention should be paid to the different responses of SAT_{MA} to the spatial distribution of the NAO at subseasonal timescales.

1. Introduction

Global surface air temperature (SAT) records exhibit a remarkable long-term warming trend. However, in recent winters, mid-latitude Asia (MA, 35° – 58° N, 65° – 120° E) has suffered more frequent extreme cold surges (Mori *et al* 2014) and SAT reversals (Li *et al* 2022b), which have serious negative consequences for human health, ecological systems and livestock husbandry (Li *et al* 2022a). During the 2015/16 boreal

winter, an unusually warm period was observed over East Asia in early winter, and an extreme cold wave was recorded in mid-late January, with SAT differences between early and late winter of up to $6.5\text{ }^{\circ}\text{C}$ (Geng *et al* 2017). The winter of 2020/21 showed a significant reversal from cold to warm in East Asia, with a maximum SAT difference of $18\text{ }^{\circ}\text{C}$ (Yang *et al* 2022). This subseasonal reversal of SAT can end the dormancy period of crops, freeze vegetables and cause damage to infrastructure (IPCC 2012). In addition,

the subseasonal SAT reversals also represent a challenge in the context of short-term climate prediction (Li *et al* 2020). Therefore, subseasonal variations in the spatial and temporal distribution of SAT should be investigated to improve its predictability.

Previous studies have revealed that the variation of winter SAT anomalies over MA is largely controlled by the large-scale atmospheric circulation at mid–high latitudes (Li *et al* 2022a). Two critical semi-permanent atmospheric systems over the Eurasian continent play important roles in linking climate variations in the Arctic and Eurasia: the Siberian high (SH) and the Ural blocking high (UBH) (Cohen *et al* 2001, Cheung *et al* 2012). The frequency of cold-wave conditions in East Asia is positively correlated with the intensity of the SH (Ding *et al* 1990). An enhanced SH may contribute to an outbreak of cold-wave events over MA via related changes in radiation conditions and heat budgets (Cohen *et al* 2001, Gong and Ho 2002). The quasi-biweekly warm Arctic–cold Eurasia anomaly will be stronger when associated with the UBH (Luo *et al* 2016). In addition, the effects of the development and decay of the UBH are not limited to the direction of the trough downstream—they are also strongly linked to the evolution of the SH and cold-wave events (Peng *et al* 2022). Persistent strengthening of the UBH and SH and northerly winds ahead are key drivers of enhanced cold advection (Zhou *et al* 2009, Liu *et al* 2019), which can lead to the continued presence of a cold anomaly in MA. In contrast, when the UBH and SH show subseasonal out-of-phase changes during the winter, a corresponding reversal of SAT also occurs (Yan *et al* 2022, Yu *et al* 2022).

The North Atlantic Oscillation (NAO) has long been recognized as a key factor in the winter SAT variation over Eurasia (Trigo *et al* 2002). Previous studies have also found that the NAO can influence SAT variation by regulating the frequency of cold air bursts (Hurrell and Van Loon 1997). In the positive phase of the NAO, the strengthened westerly wind field guides warm air to MA, resulting in a warm anomaly (Trigo *et al* 2002). However, research has also shown that the effects of the NAO are complex and are related not only to the NAO phase but also to its spatial distribution. Different combinations of the NAO and the East Atlantic pattern or the Scandinavia teleconnection (SCAND) correspond to different temperature, precipitation, and wind speed responses across Europe (Comas-Bru *et al* 2014). Eastward shift of the NAO could affect the number of deep cyclones, near-surface air temperature and turbulent surface heat flux (Jung *et al* 2003). In the summer, this shift also favors rainfall over East Asia during the positive phase (Sun and Wang 2012, Du *et al* 2020).

Previous studies have focused on the influence of atmospheric circulations, such as the NAO, SH

and UBH on average winter SAT anomalies over MA, and the mechanisms via which these influences occur. However, SAT in MA exhibits significant subseasonal variations in winter (Yang and Fan 2022, Li *et al* 2022a), which may lead to extreme climate events. For example, the significant SAT reversal from cold to warm in winter 2020 was conducive to the occurrence of sandstorms in the following spring (Yin *et al* 2022). Recent studies have demonstrated that a rapid subseasonal reversal of NAO phase can lead to SAT reversal (Geng *et al* 2017), but the relationship between changes in the spatial distribution of the NAO and SAT anomalies remains unclear. In this article, we aim to highlight the subseasonal variability of SAT in MA and associated atmospheric circulation, and to further clarify the role of the spatial distribution of the NAO.

2. Data and methods

2.1. Data

Daily meteorological data for winter (December–February) over the period 1979–2021 were obtained from ERA5, including 2 m temperature, sea level pressure (SLP), geopotential height at 500 hPa (Z500), winds at 850 hPa (UV850) and zonal wind at 200 hPa (U200). The daily SAT site observations (OBS) over the period 1979–2021 were obtained from the Global Historical Climatology Network daily (GHCNd) from a total of 1550 sites. Simulation data from 35 historical experimental models (table S1) from the sixth phase of the Coupled Model Intercomparison Project (CMIP6) for winter over the period 1979–2013 were also used (Eyring *et al* 2016).

The daily NAO and monthly SCAND indices for winter over the period 1979–2021 were obtained from the National Oceanic and Atmospheric Administration Climate Prediction Center. The SH index is defined as the area-averaged SLP over central Siberia (40°–60° N, 70°–120° E) and the UBH index is defined as the regional average of Z500 within the region of (50°–70° N, 40°–80° E) (Yan *et al* 2022). The 850 hPa meridional wind index (V850) is defined as the regional average of meridional wind over MA. The NAO_W index is defined as the difference in SLP between the northern center (65°–77° N, 5°–35° W) and the southern center, which was located over the Atlantic (35°–50° N, 55°–25° W). The NAO_E index is defined as the difference in SLP between the northern center and the southern center, which was located over Western Europe (35°–50° N, 15° W–15° E). All the data and indices in this study were removed the daily linear trends on each day separately before use.

2.2. Methods

Season-reliant empirical orthogonal function (S-EOF) analysis was used in this study to assess

the year-to-year variation of winter SAT in MA, and its subseasonal evolution in particular. The derived spatial patterns for each S-EOF mode contained two sequential patterns representing the subseasonal evolution of the SAT. They share the same yearly value in their corresponding normalized time series of the standardized principal component (PC) (Wang and An 2005).

Horizontal wave activity fluxes (WAF) were computed to analyze the propagation of Rossby waves, based on the equations generalized by Plumb (1985):

$$\text{WAF} = p \cos \varphi \left\{ \begin{array}{l} v'^2 - \frac{1}{2\Omega \sin 2\varphi} \frac{\partial(v'\Phi')}{\partial \lambda} \\ -u'v' + \frac{1}{2\Omega \alpha \sin 2\varphi} \frac{\partial(u'\Phi')}{\partial \lambda} \end{array} \right\}$$

where p is air pressure, u and v represent zonal and meridional winds, Φ is geopotential height, Ω is the Earth's rotation rate, α is the Earth's radius, and φ and λ are latitude and longitude, respectively.

3. Subseasonal reversal of SAT variability over mid-latitude Asia

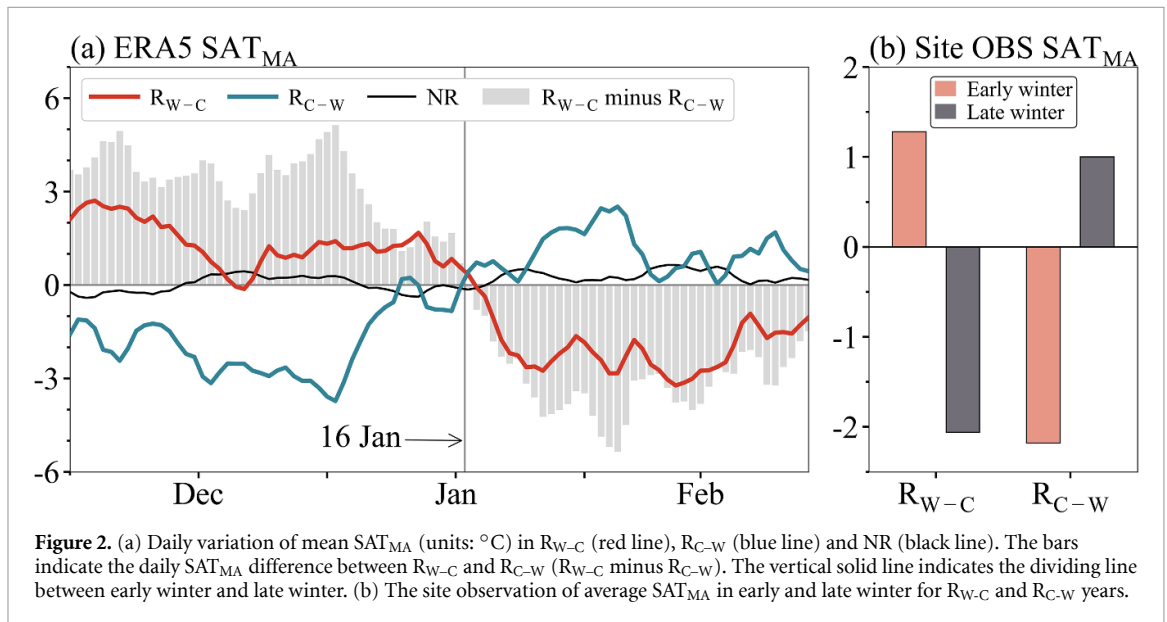
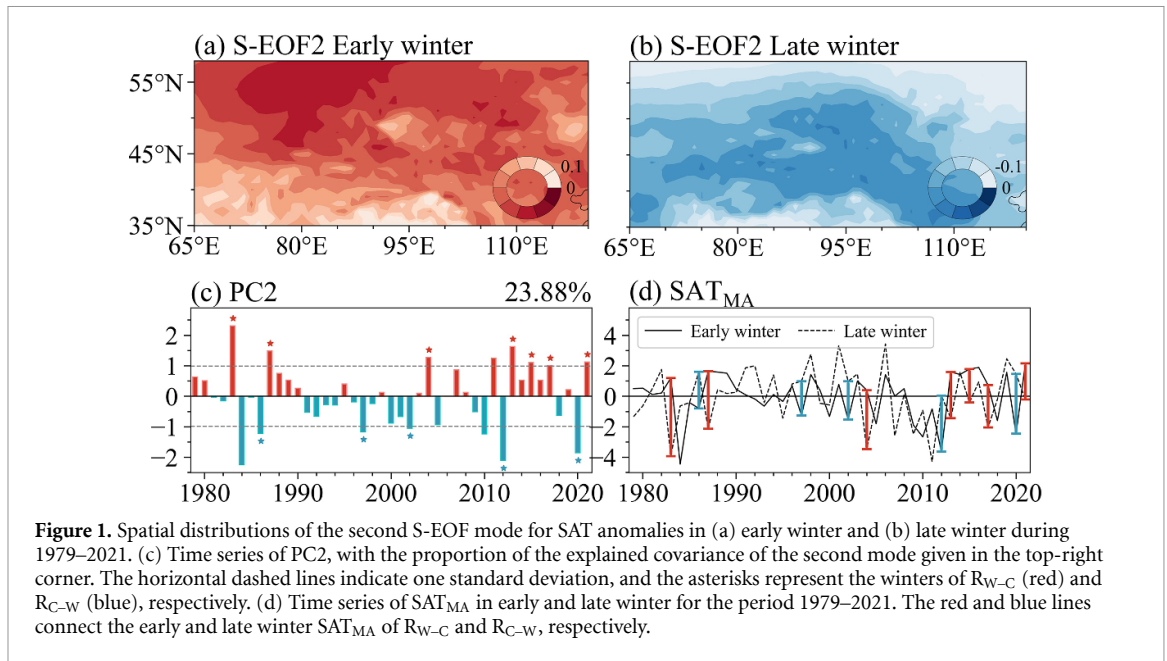
The daily evolution of area-average SAT anomalies over MA (SAT_{MA}) in winters over the period 1979–2021 showed that the average subseasonal reversal point was 16 January (not shown). For example, the winter of 2020 showed a persistent cold anomaly before 16 January and a persistent warm anomaly after this date, with an average shift in SAT_{MA} from -2.5 °C to 1.5 °C (figure S1). The abrupt change characteristic of the SAT reversal was clearly evident in the latitude–time profile (figure S2), indicating that 16 January was the time point at which the reversal occurred. Winter can therefore be divided into two periods: early winter (1 December to 16 January) and late winter (17 January to 28 February).

The first two leading S-EOF modes of early and late winter SAT in MA were separable and well distinguished from each other. In the first mode, a consistent SAT anomaly was observed for early and late winter (figure S3). This means that the whole winter will be warmer or colder than usual. In contrast, in the second mode, the SAT exhibited a reversal between early and late winter (figures 1(a) and (b)). The correlation coefficients between the standardized second principal component (PC2) and SAT_{MA} for early and late winter were 0.79 and -0.48 , respectively, both of which were higher above the 95% significance level. Based on PC2 and daily SAT_{MA} , the winters during 1979–2021 can be divided into three categories: ‘warm to cold’ reversal (R_{W-C}), ‘cold to warm’ reversal (R_{C-W}) and ‘no reversal’ (NR). R_{W-C}/R_{C-W} were defined as the winters for which the standardized PC2 was above 1/below -1 standard deviation and the SAT_{MA} in early and late winter was

reversed (figure 1(c)). For R_{W-C} and R_{C-W} , there was a marked opposite in SAT_{MA} between early and late winter (figure 1(d))—a consistent finding that was not caused by extreme values—while NR showed a small fluctuation (figure 2(a)). Calculations of R_{W-C} minus R_{C-W} showed that SAT_{MA} exhibits a persistent warm anomaly in early winter and a persistent cold anomaly in late winter. However, the intensity of the cold anomalies in R_{W-C} and R_{C-W} was more significant than that of the warm anomalies; the site OBS also showed the same results (figure 2(b)).

In the R_{W-C} winter, SAT over MA exhibited a positive anomaly ($\text{SAT}_{\text{MA}} = 1.36$ °C) in early winter and a negative anomaly ($\text{SAT}_{\text{MA}} = -1.94$ °C) in late winter (figures 3(a) and (b)). In contrast, R_{C-W} showed a reversal from negative to positive (-1.93 °C in early winter and 1.02 °C in late winter) (figures 3(c) and (d)). The spatial distribution of SAT was not the same for early and late winter in both R_{W-C} and R_{C-W} . In early winter, the SAT anomaly showed a consistent variation throughout the whole of Eurasia, with maximum values appearing in the northwest of MA (figures 3(a) and (c)). However, in late winter, the SAT anomaly was characterized by a dipole pattern similar to warm Arctic–cold Eurasia (Zhang *et al* 2021), with two anomaly centers over the Arctic and MA (figures 3(b) and (d)). The maximum value of the SAT anomaly occurred in the center of MA. Differences in the spatial distribution between early and late winter SAT anomalies were also observed in the site OBS data (figure S4), which suggested that different physical mechanisms may modulate the changes of SAT in early and late winter. In addition, in reversed winters, late winter SAT_{MA} was often significantly correlated with SAT in eastern China, which means that if the reversal in late winter cannot be predicted, the signal in eastern China may also be missed.

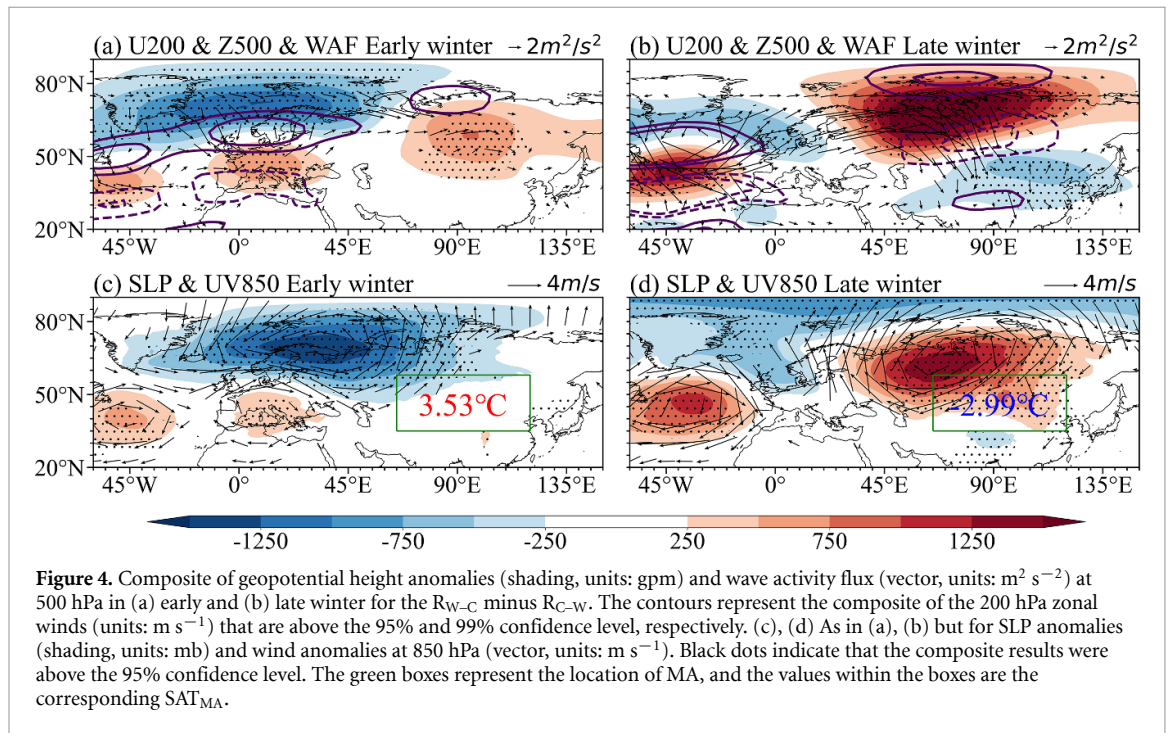
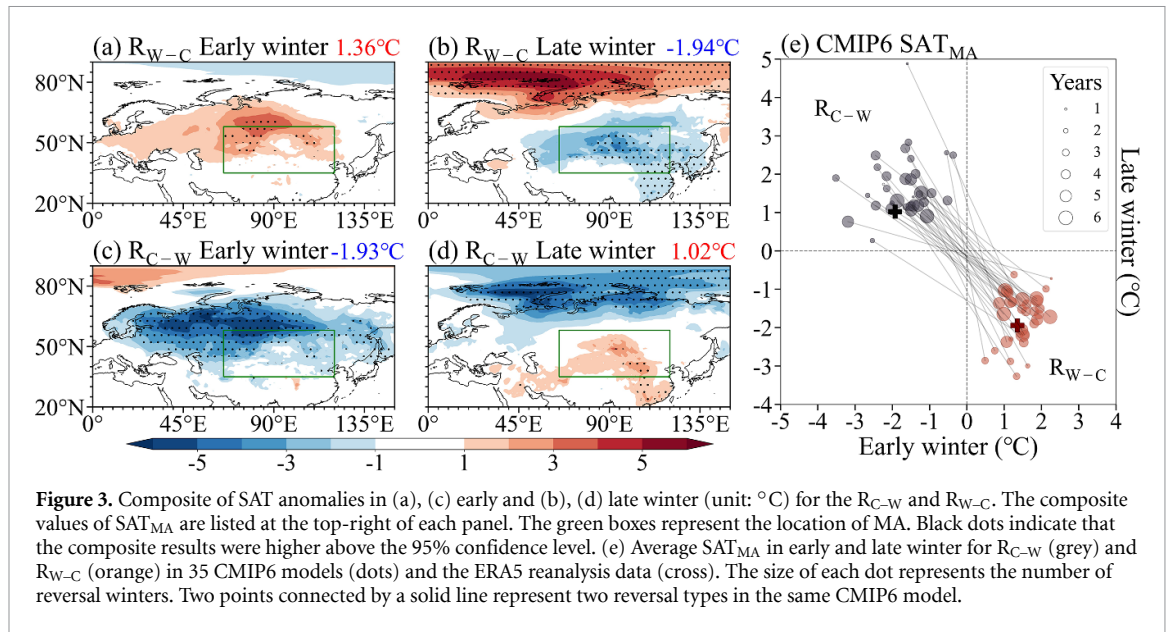
The same criteria were used to analyze the winters for each CMIP6 model, and the SAT_{MA} values in early and late winter for the R_{W-C} and R_{C-W} were calculated (figure 3(e)). For all CMIP6 models, the average difference between early and late winter SAT_{MA} was found to be 3.22 °C for R_{W-C} and -3.40 °C for R_{C-W} . These values are close to those from the ERA5 reanalysis data (3.30 °C and -2.95 °C). However, the ability of different models to capture SAT_{MA} reversals varies significantly, with the best-performing models able to capture 11 winters and the worst-performing models managing to capture only one (table S1). The vast majority of models were able to capture SAT_{MA} reversals of five winters or more, but only eight models were able to capture a comparable proportion of reversed winters to ERA5 (i.e. >10). In other words, although every model could capture the reversal of SAT_{MA} , the number of years of reversal captured was generally small and the simulation ability varies greatly between models.



4. Relationship between atmospheric circulation and the subseasonal reversal

Corresponding to the reversal of SAT_{MA} , the key atmospheric circulation characteristics from the lower to the upper troposphere during R_{W-C} and R_{C-W} also differ significantly between early and late winter (figures S5 and S6). The differences in atmospheric circulations between R_{W-C} and R_{C-W} winters were very similar to the spatial distribution of R_{W-C} and R_{C-W} , confirming the need to further analyze the differences between R_{W-C} and R_{C-W} (figure 4). For ease of description, the subsequent analyses were based on the difference between R_{W-C} and R_{C-W} (i.e. R_{W-C} minus R_{C-W}).

In early winter, the zonal wind at 200 hPa exhibited a positive/negative pattern of anomalies from north to south over the North Atlantic (figure 4(a)), which corresponded well to the geopotential height anomaly at 500 hPa. The strong WAF over the North Atlantic coincided with a meridional dipole pattern in the geopotential height. In addition, the WAF propagates eastward from the Atlantic to MA, exciting a zonal wave train pattern characteristic of the negative phase of SCAND (figure 4(a)). The eastward extension of the North Atlantic jet stream (NAJS) enhanced the anticyclonic circulation anomaly over northern China (Du *et al* 2020) and, as one center of SCAND, blocked the southward movement of cold polar air, resulting in a warm anomaly in MA.



At this point, SCAND was the dominant middle troposphere teleconnection that affected early winter SAT, and the correlation coefficient between PC2 and SCAND ($CC = -0.76$) was significantly higher than that of UBH ($CC = -0.25$) (figure 5(a)). The SLP anomalies exhibited an NAO-like pattern, the positive anomaly showing two centers in the Atlantic Ocean and Western Europe, but the former was stronger (figure 4(c)). The negative anomaly was significantly stronger than the positive anomaly, and its eastward extension into Siberia led to a weakened SH. The accompanying strong southwest wind over Eurasia prevented the southward movement of cold air. Therefore, the co-regulation of the eastward extension of the NAJS, the negative phase of SCAND, the

weakening of UBH and SH, and the southerly winds near the surface led to the positive SAT anomaly in early winter.

In late winter, the atmospheric circulation was significantly different from those observed in early winter. The NAJS receded significantly westward relative to its position in early winter. The abnormal easterly wind over Asia shifted northward to the north of MA and intensified (figure 4(b)). This corresponded to a significant strengthening of the UBH and brought cold polar air to MA. SAT shifts from a warm anomaly in early winter to a cold anomaly in late winter, resulting in the reversal of SAT_{MA} . WAF manifests primarily as meridional transport, corresponding to a significant enhancement of the

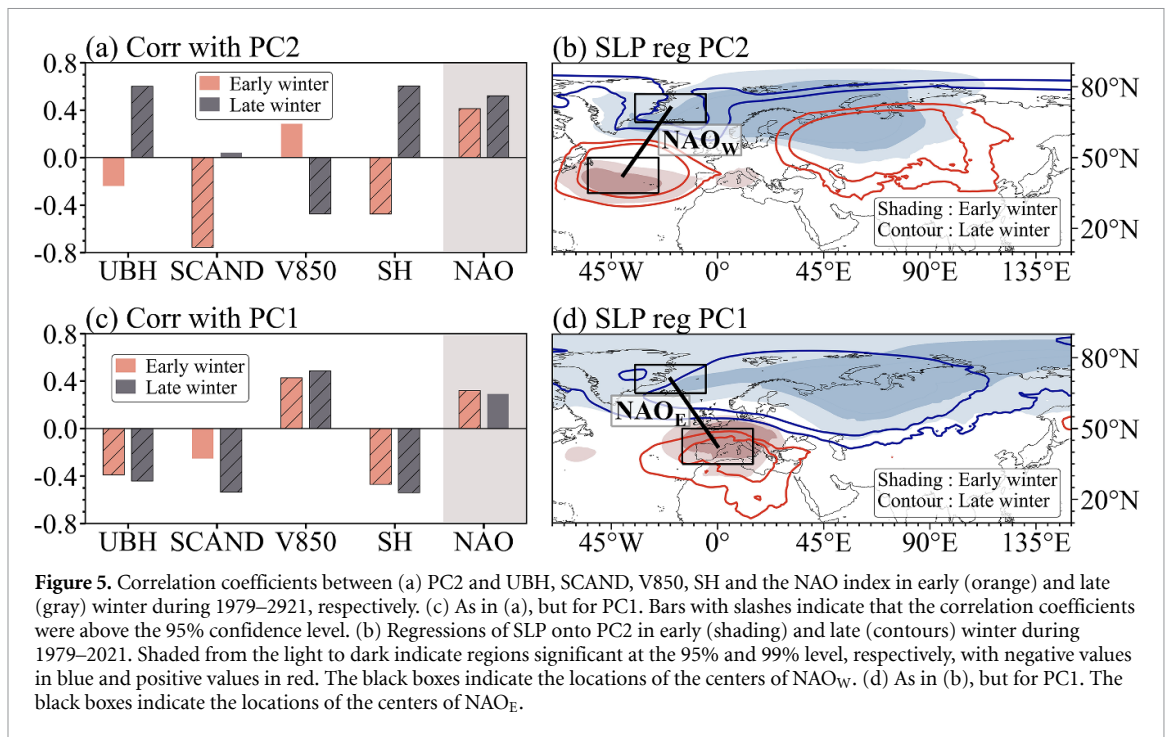


Figure 5. Correlation coefficients between (a) PC2 and UBH, SCAND, V850, SH and the NAO index in early (orange) and late (gray) winter during 1979–2021, respectively. (c) As in (a), but for PC1. Bars with slashes indicate that the correlation coefficients were above the 95% confidence level. (b) Regressions of SLP onto PC2 in early (shading) and late (contours) winter during 1979–2021. Shaded from the light to dark indicate regions significant at the 95% and 99% level, respectively, with negative values in blue and positive values in red. The black boxes indicate the locations of the centers of NAO_w . (d) As in (b), but for PC1. The black boxes indicate the locations of the centers of NAO_E .

meridional gradient of the atmospheric circulation in the middle troposphere. Cold advection in the Arctic and the warm advection in Eurasia led to a meridional dipole anomaly in SAT in late winter. In addition, SCAND was no longer the dominant mode in late winter, and the correlation coefficient with PC2 was only 0.04 (figure 5(c)). The UBH became the dominant middle troposphere atmospheric system affecting SAT_{MA} ($CC = 0.54$). This finding is also supported by the results of a previous study, which demonstrated that the formation of dipole patterns over the Arctic–Eurasia region may be related to the UBH (Li and Fan 2022b). Near the surface, a significantly enhanced SH is accompanied by strong northerly winds formed over Eurasia (figure 4(d)), bringing cold advection to MA.

In short, the reversal of SAT_{MA} was associated with changes in the atmospheric circulation anomalies in late winter relative to early winter. However, it is noteworthy that the phase of the NAO did not show the expected opposite sign, but the spatial distribution of the NAO in late winter was different from that of early winter. In late winter, the negative northern center of action was weakened, while the positive southern center shifted westward and strengthened significantly.

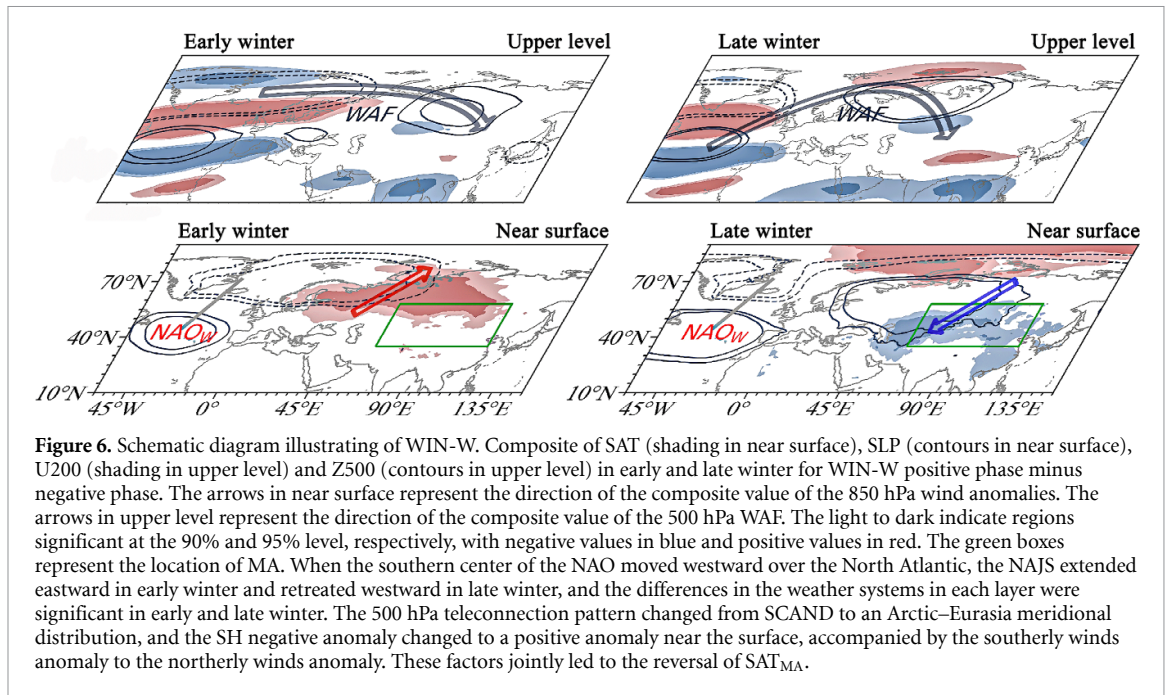
This reversal of the atmospheric circulation can also be reproduced by the CMIP6 models. Taking the SH as an example, in more than 85% of CMIP6 models, the SH index showed the opposite sign when the SAT_{MA} was reversed (figure S7). However, the model simulations underestimated the strength of the SH, especially in late winter. Only two models were able to match the differences between R_{W-C} and R_{C-W} that

were observed in the ERA5. Moreover, CMIP6 models could not simulate the asymmetry of SH intensity in early and late winter. Therefore, although CMIP6 models can simulate the sign reversal of the SH, its intensity is poorly simulated.

5. Impact of the westward shift of the NAO

The SAT_{MA} reversal was associated with significant differences in atmospheric circulation. Between the early and late winter, correlation coefficients between PC2 and UH, SCAND, V850 and SH were of the opposite sign, but were all positive between NAO and PC2, which instead of the expected contrary (figure 5(a)). This raises the question of why the same NAO phase causes SAT reversal. In addition, the correlation between PC1 (persistent SAT anomaly over MA) and the NAO also shows the same positive sign in early and late winter (figure 5(c)). Why are the effects of the NAO on SAT_{MA} so diverse? And by what mechanism do these effects occur?

Previous studies have shown that SAT is sensitive not only to the phase of the NAO, but also to the exact location of the NAO centers (Castro-Díez *et al* 2002). Therefore, it was speculated that changes in the spatial distribution of the NAO lead to the different SAT_{MA} responses. Some studies have demonstrated that the southern center of the NAO shows obvious meridional position difference, sometimes shifting more than 35° in longitude (Peterson *et al* 2003). This significant east–west shift may account for the different effects of the NAO. Hereafter, the NAO with its southern center shifting westward and located over the North Atlantic is referred to as NAO_w (figure 5(b)),

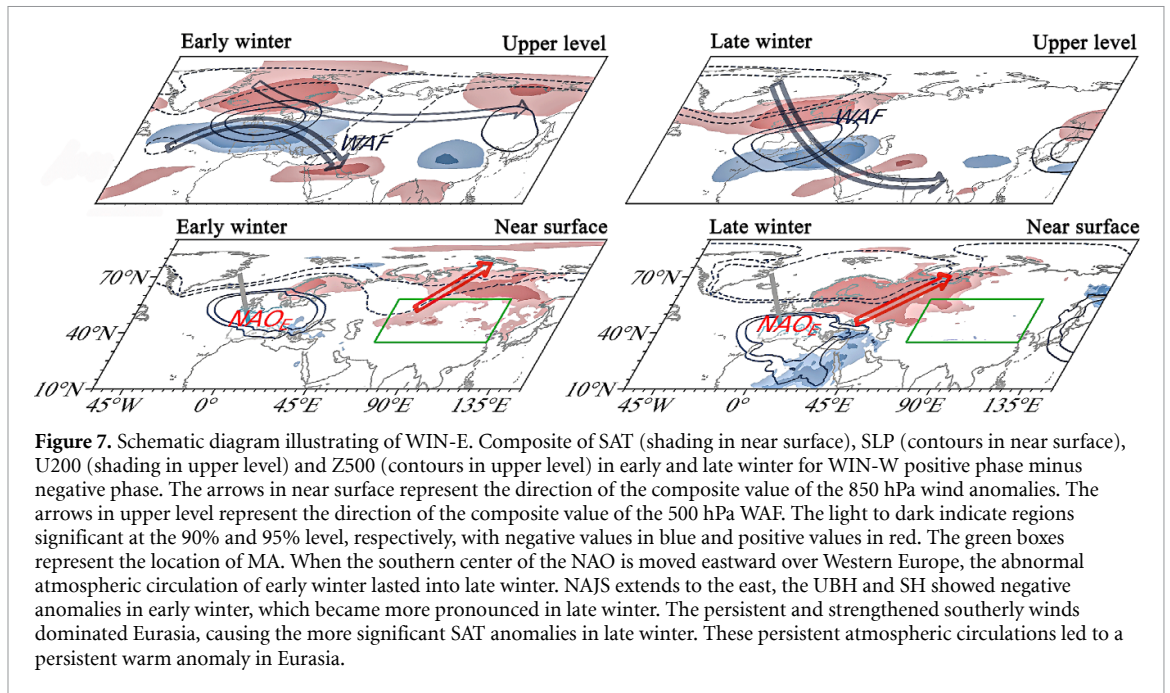


south center shift eastward and located over Western Europe is referred to as NAO_E (figure 5(d)). The northern centers of both NAO_W and NAO_E are located near Iceland, which is the average location of the climate. The partial correlation between PC2 and the NAO_W (0.20 in early winter, 0.58 in late winter) was significantly higher than that of the NAO_E (0.06 in early winter, -0.13 in late winter), especially in late winter, indicating that the reversal of SAT_{MA} was largely due to the NAO_W . In contrast, the persistent SAT anomalies were mainly affected by the NAO_E , and the partial correlation between PC1 and the NAO_E (0.40 in early winter, 0.38 in late winter) was higher than that of the NAO_W (-0.16 in early winter, -0.10 in late winter). Regression of SLP onto PC1 and PC2 also confirmed the different responses of SAT to different spatial distributions of the NAO (figures 5(b) and (d)), that is, persistent SAT_{MA} corresponds to the NAO_E and SAT_{MA} reversal corresponds to the NAO_W .

In winters with opposite NAO phases in early and late winter, SAT was influenced by both the phase and spatial distribution of the NAO, and most of them were weak or of unclear type in early or late winter (figure not shown). Therefore, this paper focuses more on the effect of the spatial distribution of the NAO and does not consider winters with reversed NAO phases (table S2). Under the premise that the NAO phase was unchanged in early and late winter, winters were divided into four categories according to the relative strength of NAO_W and NAO_E index: WIN-W (NAO_W for early and late winter), WIN-E (NAO_E for early and late winter), WIN-WE (NAO_W for early winter and NAO_E for late winter) and WIN-EW (NAO_E for early winter and NAO_W for late winter). Of these four winter types, SAT reversal

occurs more often during WIN-W and WIN-EW, both of which show the NAO_W in late winter. Nine SAT_{MA} reversal winters showed the same NAO phase in early and late winter, eight of which were WIN-E or WIN-WE (tables S3(a) and (b)). SAT_{MA} reversals were observed in more than 60% of WIN-W and WIN-EW winters, and most positive (negative) NAO winters exhibit R_{W-C} (R_{C-W}). In some WIN-W and WIN-EW winters, such as 1984 and 2011, there was no change in the sign of SAT_{MA} between early and late winter, but the degree of variation in SAT_{MA} was large and was comparable with that of reversal winters. In contrast, all of the WIN-E winters and half of WIN-WE winters exhibited persistent SAT_{MA} anomalies (tables S3(c) and (d)), and most positive (negative) phase winters show continuous warm (cold) anomalies.

In WIN-W (positive phase minus negative phase) winters, most of which showed an SAT_{MA} reversal, the atmospheric circulation showed similar characteristics to those of SAT_{MA} reversal years (figure 6). The increasing zonal wind and eastward extension of NAJS in early winter favors barotropic kinetic energy conversion to seasonal kinetic energy, thus providing adequate kinetic energy for cyclonic eddy growth (Du et al 2020). Warm and moist air in front of the trough transported from the North Atlantic Ocean to Eurasia, and the air column over Siberia was heated, causing the weakening of the SH. In late winter, the NAJS westward receded, reducing the eastward movement of the cyclone, which was not conducive to the transport of warm and moist air over the North Atlantic. In addition, the ridge near the Ural Mountains facilitated the formation of the blocking, and the anomaly anticyclone enhanced the northerly surface winds and lead to cold air accumulation over Siberia,



resulting in an enhanced SH (Ma *et al* 2018). The geopotential height in the middle troposphere changed from a positive anomaly over Eurasia to an Arctic–Eurasia meridional distribution with the strengthening of the UBH. The SH showed a negative anomaly in early winter and a positive anomaly in late winter, resulting in the wind anomaly over MA changing from a southerly wind before the trough to a northerly wind before the ridge. Together, these variations led to a very significant subseasonal reversal of SAT_{MA} from a positive anomaly ($SAT_{MA} = 2.02\text{ }^{\circ}\text{C}$) in early winter to a negative anomaly ($SAT_{MA} = -2.14\text{ }^{\circ}\text{C}$) in late winter (figure 6). The spatial distribution of SAT anomalies was also consistent with that of SAT_{MA} reversal winters (figure 3). For WIN-EW, the atmospheric circulation characteristics were largely the same as those of WIN-W, with SH, UBH and surface wind reversals in early and late winter, leading to the reversal of SAT_{MA} ($5.23\text{ }^{\circ}\text{C}$ in early winter and $-0.84\text{ }^{\circ}\text{C}$ in late winter) (figure S8).

In WIN-E, which showed a persistent SAT_{MA} in most winters, the characteristics of atmospheric circulation in early winter lasted into late winter (figure 7). A continuous eastward extension of the NAJS resulted in negative anomalies of the UBH and SH and were stronger in late winter. Persistent and strengthened southerly winds dominated Eurasia, causing more significant SAT anomalies in late winter. These persistent atmospheric circulations resulted in a warm anomaly over MA throughout the whole winter ($1.51\text{ }^{\circ}\text{C}$ in early winter and $1.67\text{ }^{\circ}\text{C}$ in late winter) (figure 7). The warm anomaly in early winter was mainly located over northeast MA, and in late winter was observed over Europe and northwest MA. For WIN-WE winters, there was no change

in sign for SAT_{MA} and an increase from $0.54\text{ }^{\circ}\text{C}$ in early winter to $2.80\text{ }^{\circ}\text{C}$ in late winter was observed (figure S9).

6. Conclusion and discussion

In this study, winter SAT reversal over MA was studied at the daily scale. Season-reliant empirical orthogonal function analysis of early and late winter showed that SAT reversal over MA occurred in the second mode (figures 1(b) and (d)). Persistent SAT_{MA} anomalies and significant changes in sign between early and late winter were observed for both R_{W-C} and R_{C-W} (figure 2). The characteristics of the atmospheric circulations for R_{W-C} minus R_{C-W} showed clear differences between early and late winter. In early winter, the NAJS extended eastward and the middle troposphere was largely controlled by SCAND. The lower troposphere was characterized by a negative SH anomaly and a strong southerly wind anomaly (figures 4(a) and (c)), leading to a positive SAT_{MA} anomaly. In late winter, the NAJS moved westward, and the middle troposphere was mainly controlled by the UBH and exhibited an Arctic–Eurasia meridional distribution. The lower troposphere showed a significant positive SH anomaly and a northerly wind anomaly (figures 4(b) and (d)), resulting in a negative SAT_{MA} anomaly. In combination, the above factors led to the reversal of SAT between early and late winter (figures 3(a)–(d)).

More importantly, the relationship between the spatial distribution of the NAO and the reversal of the SAT anomaly was explored. It was found that SAT reversal was more likely to occur when the south center of NAO shifts westward, and when the south

center of NAO shifts eastward the SAT will be persistent (figures 5(b) and (d)). In this article, winters were divided into four categories: WIN-W, WIN-E, WIN-WE and WIN-EW. In WIN-W and WIN-EW, changes in atmospheric circulation were similar to those observed in SAT_{MA} reversal winters: between the early and late winter SH, the UBH and surface wind reversals were observed, leading to the reversal of SAT_{MA} (figures 6 and S8). In WIN-E and WIN-WE, the atmospheric circulation in early winter lasted into late winter (figures 7 and S9). Further strengthening of the UBH and SH in late winter resulted in a continuously increasing warm anomaly over MA.

The results presented here show that different NAO spatial distributions correspond to different atmospheric circulations in early and late winter, but how NAO causes the change of atmospheric circulation is worthy of further study. The relationship between SAT reversal and the NAO has also been analyzed based on the CMIP6 models, but the relationship is not well demonstrated. In 80% models, WIN-W and SAT reversals co-occurred in less than three winters. There are two possible reasons for the discrepancy between the CMIP6 models and ERA5 results. First, the models themselves are poor at simulating SAT reversal. Second, the NAO prediction skill of the models is limited to subseasonal timescales, particularly in terms of their spatial distribution (Johansson *et al* 2007). The frequency of SAT_{MA} reversal is closely related to SAT anomalies in eastern China, so it is of great significance to study and predict the reversal of SAT_{MA}. However, the effect of global warming on SAT_{MA} reversal is unclear, and the relationship between the two deserves continuous attention and research. In addition, the effects of forcing factors on SAT_{MA} were not considered, though SAT_{MA} is known to be affected by factors such as snow cover (Wu and Chen 2016), North Atlantic sea surface temperature (Chen *et al* 2021) and Arctic sea ice (Mori *et al* 2014). At the same time, the NAO is also affected by forcing factors, such as the El Niño–Southern Oscillation (Zhang *et al* 2015), snow cover (Deser *et al* 2004) and sea ice (Screen *et al* 2013). Therefore, the relationship between SAT and the NAO is complicated. In short, more factors need to be considered to fully understand the reversal of SAT anomalies over Eurasia during early and late winter and the relationship between these reversals and the spatial distribution of the NAO.

Data availability statement

Daily 2m temperature and sea level pressure can be obtained from <https://cds.climate.copernicus.eu/cdsapp#!/dataset/reanalysis-era5-single-levels?tab=form>. Daily geopotential height at 500 hPa, winds at 850 hPa and zonal wind at 200 hPa can be obtained from [https://cds.climate.copernicus.eu/cdsapp#!/dataset/reanalysis-era5-pressure-levels?](https://cds.climate.copernicus.eu/cdsapp#!/dataset/reanalysis-era5-pressure-levels?tab=form)

[tab=form](https://cds.climate.copernicus.eu/cdsapp#!/dataset/reanalysis-era5-pressure-levels?tab=form). The Global Historical Climatology Network daily average SAT (GHCNd) can be obtained from www.ncei.noaa.gov/data/global-historical-climatology-network-daily/access/. The simulation data of 46 CMIP6 models are available from <https://esgf-node.llnl.gov/search/cmip6/>. Daily NAO index can be obtained from www.cpc.ncep.noaa.gov/products/precip/CWlink/pna/nao.shtml. Monthly SCAND index can be obtained from www.cpc.ncep.noaa.gov/data/teledoc/scand.shtml.

All data that support the findings of this study are included within the article (and any supplementary files).

Acknowledgments

This research is supported by the National Natural Science Foundation of China (Grant No. 41991283).

Author contributions

Yin Z C designed the research. Song X L, Zhang Y J and Yin Z C performed research. Song X L prepared the manuscript with contributions from all co-authors.

Conflict of interest

The authors declare no conflict of interest.

References

- Castro-Díez Y, Pozo-Vázquez D, Rodrigo F S and Esteban-Parra M J 2002 NAO and winter temperature variability in southern Europe *Geophys. Res. Lett.* **29** 1–4
- Chen S, Wu R and Chen W 2021 Influence of North Atlantic sea surface temperature anomalies on springtime surface air temperature variation over Eurasia in CMIP5 models *Clim. Dyn.* **57** 2669–86
- Cheung H N, Zhou W, Mok H Y and Wu M C 2012 Relationship between Ural–Siberian blocking and the East Asian winter monsoon in relation to the Arctic Oscillation and the El Niño–Southern Oscillation *J. Clim.* **25** 4242–57
- Cohen J, Saito K and Entekhabi D 2001 The role of the Siberian high in Northern Hemisphere climate variability *Geophys. Res. Lett.* **28** 299–302
- Comas-Bru L and McDermott F 2014 Impacts of the EA and SCA patterns on the European twentieth century NAO–winter climate relationship *Q. J. R. Meteorol. Soc.* **140** 354–63
- Deser C, Magnusdottir G, Saravanan R and Phillips A 2004 The effects of North Atlantic SST and sea ice anomalies on the winter circulation in CCM3. Part II: direct and indirect components of the response *J. Clim.* **17** 877–89
- Ding Y H 1990 Build-up, air mass transformation and propagation of Siberian high and its relations to cold surge in East Asia *Meteorol. Atmos. Phys.* **44** 281–92
- Du Y, Zhang J, Zhao S and Chen H 2020 Impact of the eastward shift in the negative-phase NAO on extreme drought over northern China in summer *J. Geophys. Res. Atmos.* **125** e2019JD032019
- Eyring V, Bony S, Meehl G A, Senior C A, Stevens B, Stouffer R J and Taylor K E 2016 Overview of the coupled model intercomparison project phase 6 (CMIP6) experimental design and organization *Geosci. Model. Dev.* **9** 1937–58
- Geng X, Zhang W, Stuecker M F and Jin F 2017 Strong sub-seasonal wintertime cooling over East Asia and

- Northern Europe associated with super El Niño events *Sci. Rep.* **7** 3770
- Gong D and Ho C 2002 The Siberian high and climate change over middle to high latitude Asia *Theor. Appl. Climatol.* **72** 1–9
- Hurrell J W and Van Loon H 1997 Decadal variations in climate associated with the North Atlantic Oscillation *Clim. Change* **36** 301–26
- IPCC (Intergovernmental Panel on Climate Change) 2012 Managing the risks of extreme events and disasters to advance climate change *Summary for Policymakers* ed C B Field et al (Cambridge: Cambridge University Press) pp 3–21
- Johansson Å 2007 Prediction skill of the NAO and PNA from daily to seasonal time scales *J. Clim.* **20** 1957–75
- Jung T, Hilmer M, Ruprecht E, Kleppek S, Gulev S K and Zolina O 2003 Characteristics of the recent eastward shift of interannual NAO variability *J. Climate* **16** 3371–82
- Li H S and Fan K 2022b Dominant patterns of winter surface air temperature over central Asia and their connection with atmospheric circulation *Atmos. Ocean. Sci. Lett.* **15** 100210
- Li H S, Fan K, Li H and Xu Z Q 2022a Impacts of central tropical pacific SST on the reversal of December and January surface air temperature anomalies over central Asia *Front. Earth Sci.* **10** 873040
- Li H, Fan K, He S P, Liu Y, Yuan X and Wang H J 2020 Intensified impacts of central pacific ENSO on the reversal of December and January surface air temperature anomaly over china since 1997 *J. Clim.* **34** 1601–18
- Liu B and Zhu C 2019 Diverse impacts of the Siberian high on surface air temperature in Northeast China during boreal winter *Int. J. Climatol.* **40** 594–603
- Luo D H, Xiao Y Q, Diao Y N, Dai A G, Simmonds I and Franzke C L E 2016 Impact of Ural blocking on winter warm Arctic–cold Eurasian anomalies. part II: the link to the North Atlantic Oscillation *J. Clim.* **29** 3949–71
- Ma S M, Zhu C W, Liu B Q, Zhou T J, Ding Y H and Orsolini Y J 2018 Polarized response of East Asian winter temperature extremes in the Era of Arctic warming *J. Clim.* **31** 5543–57
- Mori M, Watanabe M, Shiogama H, Inoue J and Kimoto M 2014 Robust Arctic sea-ice influence on the frequent Eurasian cold winters in past decades *Nat. Geosci.* **7** 869–73
- Peng J B, Sun S Q and Chen B M 2022 Maintenance and development of the Ural high and its contribution to severe cold wave activities in winter 2020/21 *Atmos. Ocean. Sci. Lett.* **15** 100130
- Peterson K A, Lu J and Greatbatch R J 2003 Evidence of nonlinear dynamics in the eastward shift of the NAO *Geophys. Res. Lett.* **30** 2002GL015585
- Plumb R A 1985 On the three-dimensional propagation of stationary waves *J. Atmos. Sci.* **42** 217–29
- Screen J A, Simmonds I, Deser C and Tomas R 2013 The atmospheric response to three decades of observed Arctic sea ice loss *J. Clim.* **26** 1230–48
- Sun J Q and Wang H J 2012 Changes of the connection between the summer North Atlantic Oscillation and the East Asian summer rainfall *J. Geophys. Res.* **117** 2012JD017482
- Trigo R M, Osborn T J and Corte-Real J M 2002 The North Atlantic Oscillation influence on Europe: climate impacts and associated physical mechanisms *Clim. Res.* **20** 9–17
- Wang B and An S 2005 A method for detecting season-dependent modes of climate variability: S-EOF analysis *Geophys. Res. Lett.* **32** 2005GL022709
- Wu R G and Chen S F 2016 Regional change in snow water equivalent–surface air temperature relationship over Eurasia during boreal spring *Clim. Dyn.* **47** 2425–42
- Yan H M, Yuan Y, Tan G R and Zi Y C 2022 Possible impact of sudden stratospheric warming on the intraseasonal reversal of the temperature over East Asia in winter 2020/21 *Atmos. Res.* **268** 106016
- Yang H Q and Fan K 2022 Reversal of monthly East Asian winter air temperature in 2020/21 and its predictability *Atmos. Ocean. Sci. Lett.* **5** 100142
- Yin Z C, Wan Y, Zhang Y J and Wang H J 2022 Why super sandstorm 2021 in North China? *Natl. Sci. Rev.* **9** nwab165
- Yu M J, Ma S M and Zhu C W 2022 The alternating change of cold and warm extremes over north Asia during winter 2020/21: effect of the annual cycle anomaly *Geophys. Res. Lett.* **49** e2021GL097233
- Zhang W J, Wang L, Xiang B Q, Qi L and He J H 2015 Impacts of two types of La Niña on the NAO during boreal winter *Clim. Dyn.* **44** 1351–66
- Zhang Y J, Yin Z C, Wang H J and He S 2021 2020/21 record-breaking cold waves in East of China enhanced by the “warm Arctic-cold Siberia” pattern *Environ. Res. Lett.* **16** 094040
- Zhou W, Chan J C, Chen W, Ling J, Pinto J G and Shao Y 2009 Synoptic-scale controls of persistent low temperature and icy weather over Southern China in January 2008 *Mon. Weather. Rev.* **137** 3978–91